Extended Abstract for I3RC

1st Workshop, Tucson, AZ
November 1999

Howard W. Barker
Cloud Physics Research Division, AES-Downsview

Abstract

All simulations were performed using the Monte Carlo method of photon transport. For simulations with the Henyey-Greenstein scattering phase function, two versions were employed: one that used optical properties exactly as prescribed and another that used -scaled properties. It is shown that both methods yield very similar fluxes and radiances but the -scaled simulations required often 30% to 50% less CPU time. Results are shown for the square-wave cloud and the 2D cloud field derived from observations made at the Atmospheric Radiation Measurement (ARM) site in Oklahoma.

1. Model description

All results presented below were computed by a forward Monte Carlo scheme (Barker 1991; Barker and Davies 1992). In this model, the spatial dimension of grid cells can vary across a domain and the domain is plane-parallel. It computes 3D absorptances in all grid cells, distributions of fluxes at the surface and top of domain (TOD), TOD radiances in any number of angular bins, as well as true nadir and zenith radiances at the surface and TOD via the method of tracing photon trajectories at each scattering event. Either idealistic (e.g., Henyey-Greenstein or elliptic) or tabulated exact phase functions can be used. It also has the capability to compute broadband fluxes (via Fu-Liou CKD or a 0.01 micron resolution model accounting for Rayleigh, water vapour, ozone, and carbon dioxide) (Fu and Liou 1992; Barker et al. 1998). Diurnal means can be computed efficiently (via MC integration) and cyclic and reflective horizontal boundary conditions can be used. The surface is typically either Lambertian or Fresnelian but a BRDF (either from tables or computed analytically) can be used. It is forced into independent column mode by setting horizontal grid-spacings arbitrarily large. It can perform either fixed or uniform distributions of both solar azimuth and zenith angles (the latter for simulations of coarse satellite binning like ERBE). It computes direct-beam irradiances into a user-specified angular width aperature and keeps track of the number of scattering events of contributing photons.

Results for two versions of the code are shown. The first is the straight Monte Carlo. The second is again the Monte Carlo but all portions of a cloud below 1 optical depth from cloudtop had their optical properties -scaled (Joseph et al. 1976) according to

$$\tau' = \tau\,(1 - \omega g^2)$$
$$\omega' = \omega\,\frac{1 - g^2}{1 - \omega g^2}$$
$$g' = \frac{g}{1 + g}$$

where τ is optical depth, ω is single-scattering albedo, and g is asymmetry parameter. The unprimed quantities are used in the first model, while the primed quantities are used in the second.

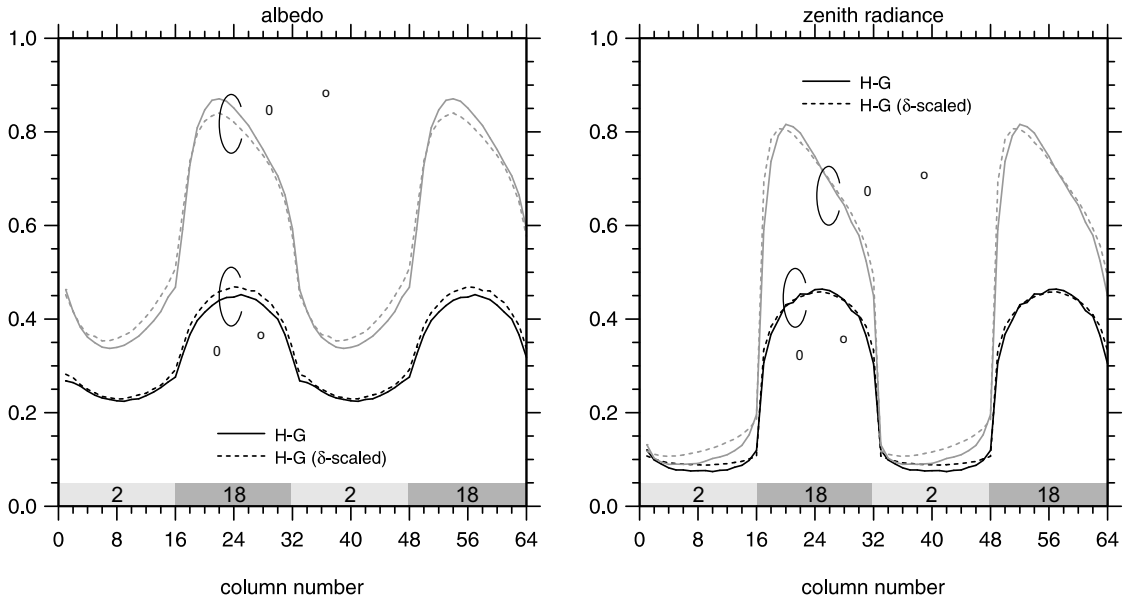

Fig. 1 Two cycles of albedo and zenith radiance at two solar zenith angles for the conservative-scattering square-wave cloud. Solid lines represent results when the Henyey-Greenstein phase function was used throughout, while dashed lines represent results when cloud beneath 1 optical depth below cloudtop were -scaled according to (1). Shaded areas at the base of the plots designate cloud optical depths.

Selected results are presented in the following sections for the square-wave cloud and the ARM-MMCR cloud.

2. Square-wave cloud

This *cloud* consists of 32 columns along the x-direction in which the first 16 have optical depth 2 while the remaining have optical depth 18.The size of the field is 0.5 km, so all columns have a width of 15.625 m. The vertical thickness of the cloud is 0.25 km everywhere (flat cloud) and the extinction coefficient is constant with height. The cloud has infinite extent in the y-direction. Each simulation was performed using 5×10^6 photons so that the top of each column received, on average, ~156,000 photons.

Figure 1 shows albedo and zenith radiance for the conservative-scattering square-wave cloud. Clearly, the -scaling has an impact, but in terms of domain averages, differences are less than 4% for albedo and 1% for zenith radiances. Similar results exist for transmitted quantities and absorptances when = 0.99.

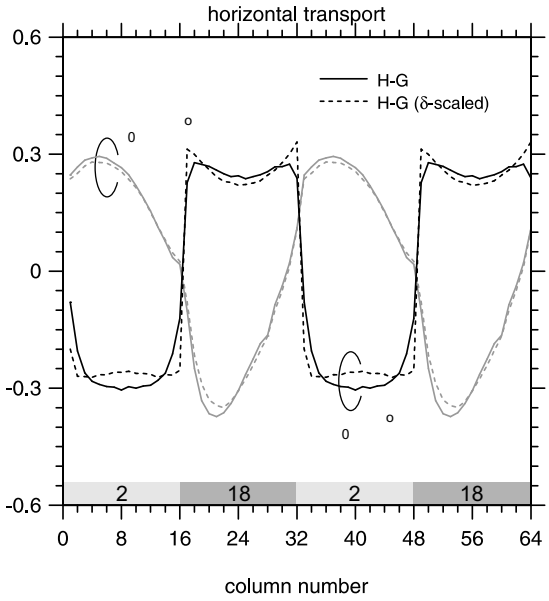

Fig. 2 As in Fig. 1 except this is for horizontal transport defined as 1 - *R* - *T* - *A*, where *R* is albedo, *T* is transmittance, and *A* (= 0) is absorptance.

Figure 2 shows the horizontal transport terms for the conservative-scattering square-wave cloud. When averaged over the domains, both models naturally produce zero net horizontal transport. There are, however, some distinct differences between the two models especially at $_0 = 60^\circ$. The -scaled version produces slightly less outflow from the central regions of both columns and slightly exaggerated horizontal transport near the transition from 2 to 18 optical depths.

3. ARM-MMCR cloud

The 2D cloud field for this experiment is based on extinction retrievals from MMCR and microwave radiometer data collected at the ARM site in Lamont, OK on Feb. 8, 1998. The field consists of 640 columns in the x-direction. The width of each column was set to 50 m (10 sec. integrations with an observed wind speed of ~5 m/s). Moreover, each column was resolved into 54 vertical layers of 45 m thick. It is assumed that the cloud is infinitely long in the y-direction.

As with the square-wave cloud, $5x10^6$ photons per simultion were used. This translates into ~7812 photons per column which is rather low. Indeed, Fig. 3 shows that while the power spectrum of total optical depth is almost scale-invariant, spectra for cloudtop albedo and zenith radiance signify essentially white noise below about 20 columns (or ~1 km). In actuality, they should be steeper than that for optical depth (Marshak et al. 1995).

Figure 4 shows the profile and vertical integral of optical depth for the MMCR cloud as well as cloudtop albedo, and cloudbase transmittance (as measured at the level housing the lowest cloudy cell. For the case of albedo at $_0 = 60^\circ$, there is a clear shift to the left of the corresponding

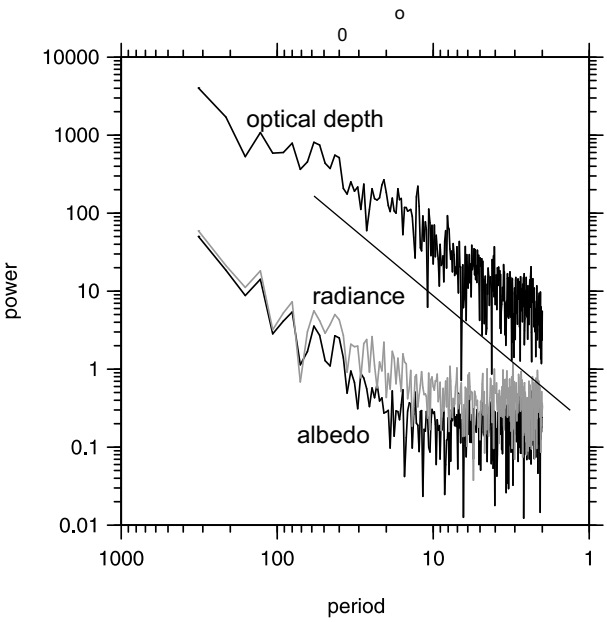

Fig. 3 Power spectra of optical depth, cloudtop albedo, and zenith radiance for the ARM-MMCR cloud in which cloud optical properties were not scaled according to (1). Straight line has a slope of -5/3.

line for $_0 = 0^\circ$. This is due to side illumination (Sun coming in from the left). This is not so notable for the transmittance plot due to heavy multiple scattering.

Figure 5 shows zenith and nadir radiances at $_0 = 60^\circ$ for the pure Henyey-Greenstein simulation plotted against those for the -scaled Henyey-Greenstein and those obtained for Deirmendjian's C1 phase function. The -scaled Henyey-Greenstein's zenith radiances are systematically greater than the unscaled Henyey-Greenstein by ~0.03. Conversely, nadir radiance differences reverse sign at intermediate values and differ on average by just 0.007.

The discrepancy between zenith radiances for the Henyey-Greenstein and C1 phase functions is largely due to random errors for the C1; domain-average values differ by less than 0.01. But, there is

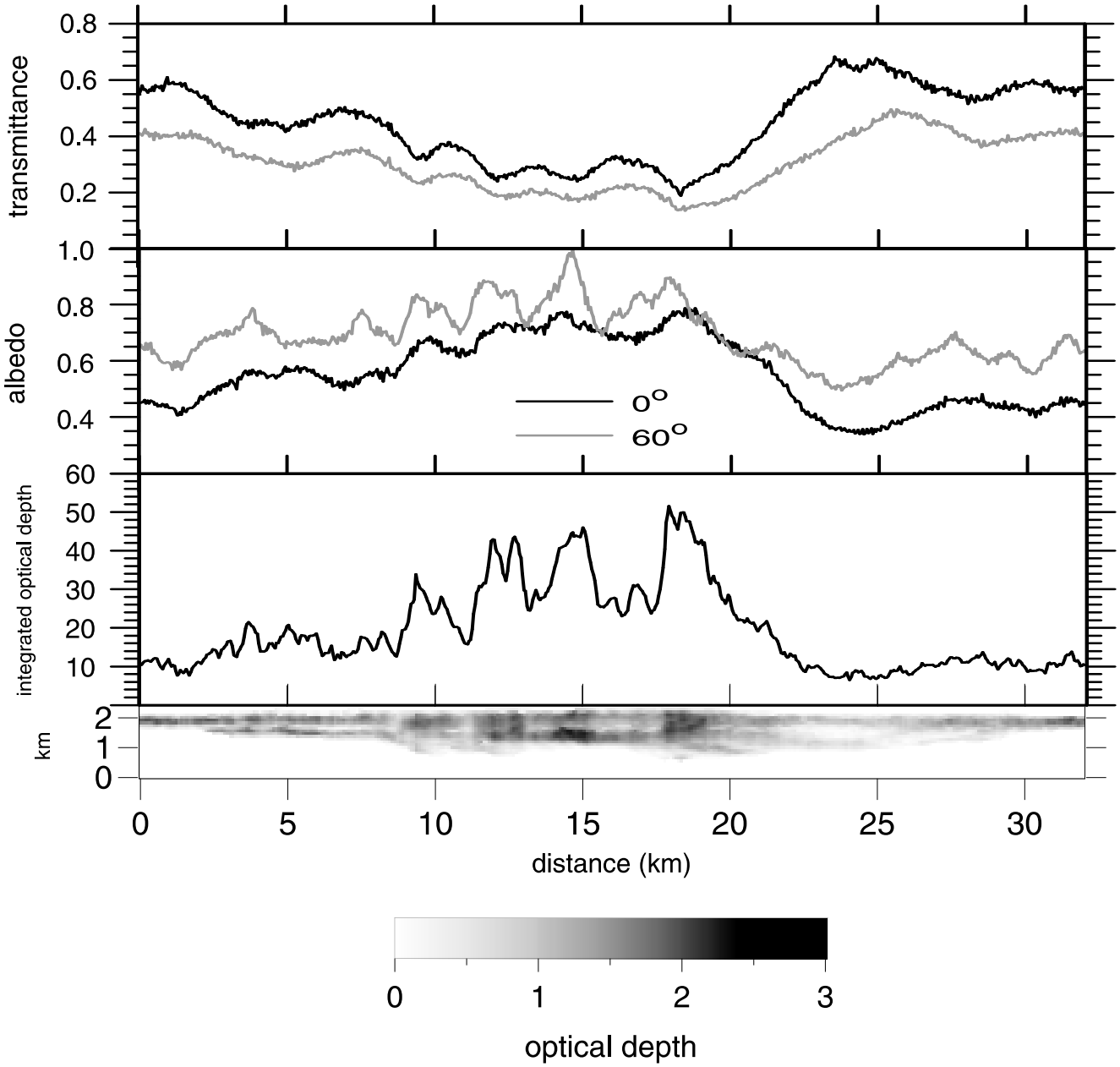

Fig. 4 Lower panel shows optical depth of each cell for the ARM-MMCR cloud. The aspect ratio of this plot is very close to that of the actual cloud. Next panel up shows the vertical integral of the lower panel (i.e., total optical depth). Upper two panels show cloudtop albedo and cloudbase transmittance for two solar zenith angles. These results are for the Monte Carlo model that did not employ the transformation listed in (1). Note the high frequency oscillations for the radiative curves (cf. Fig. 3).

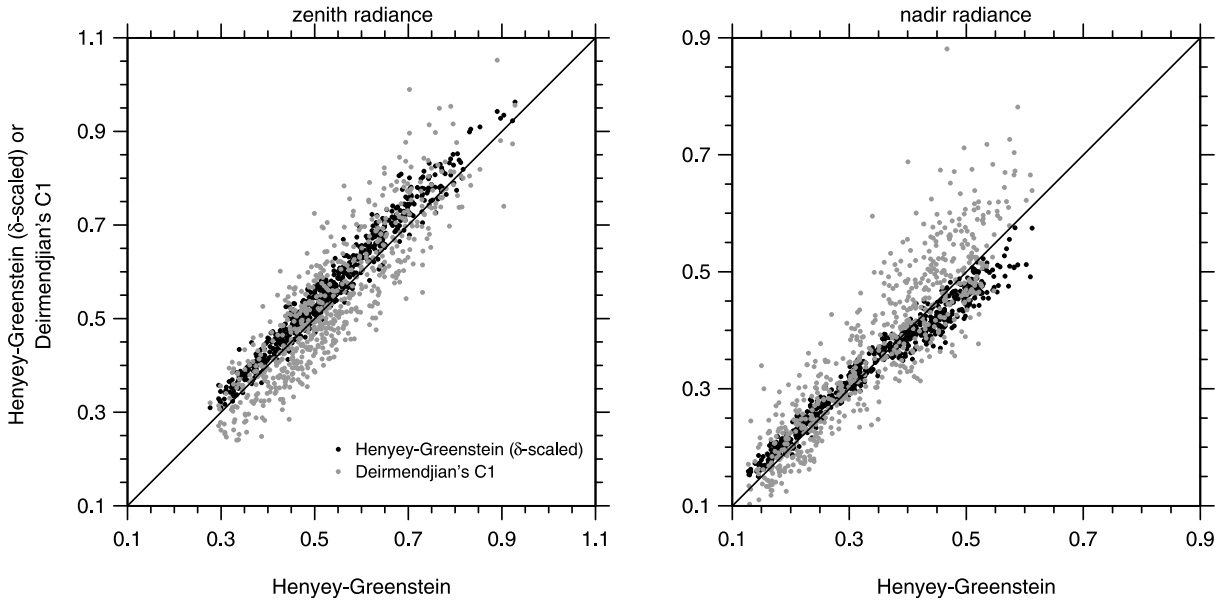

Fig. 5 Zenith and nadir radiances for the straight Henyey-Greenstein simulations plotted against corresponding values for the -scaled Henyey-Greenstain and Deirmendjian's C1 phase function. These results are for the conservative-scattering ARM-MMCR cloud (Fig. 4) at $_0 = 60^\circ$.

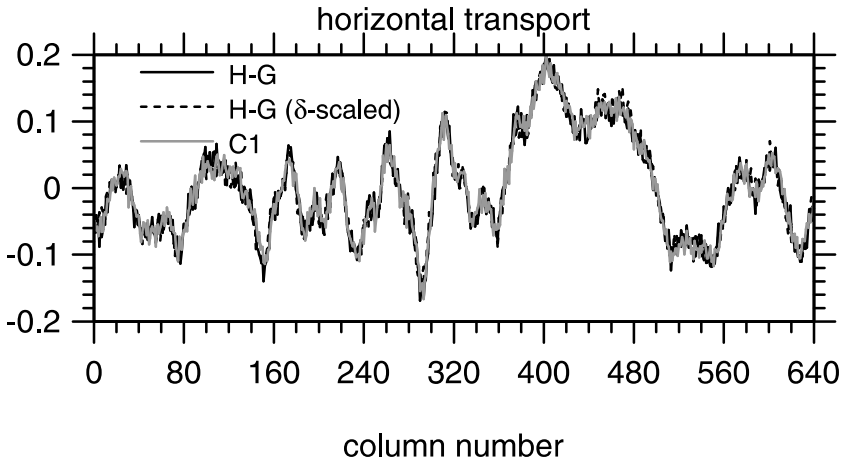

Fig. 6 Horizontal transport (see Fig. 2) for the conservative-scattering ARM-MMCR cloud (Fig. 4) at $_0 = 60^\circ$ for the three Monte Carlo simulations using different scattering phase functions.

a more pronouced bias for nadir radiance with the C1 function transmitting more, especially for thin regions. Obviously, this is due to the C1's shape forward peak which is largely obliterated in optically thick areas. Plots similar to those in Fig. 5 but for albedo and transmittance were not shown because differences were an order of magnitude smaller than those shown in Fig. 5.

Figure 6 shows series of horizontal transport for the three simulations. For this cloud field, both the phase function and the -scaling had insignificant impacts on the degree of horizontal transport.

4. Conclusion

The main purpose for performing the scaling in (1) is to save computation time. Clearly, the best time to apply this when domain-average quantities are of interest. However, as the results have shown, there is often fairly small errors incurred in distributions of both fluxes and radiances. This is rather significant as the -scaled simulations required between 50% to 70% of the CPU needed to perform the unscaled simulations. Similar savings and accuracies for the -scaled simulations were realized for the Landsat cloud field as well.

The reason why -scaling requires less CPU time is simply fewer scattering events: in the cases shown here, the optical depth of most cells is reduced by a factor of ~0.3 for the -scaled simulations. Note that while repeated applications of (1) reduces CPU usage only slightly (by about an additional 10% for infinitely many applications... the isotropic approximation), it does so at the expense of error enhancement (especially at low Sun).

Acknowledgements: I am grateful to the organizers of I3RC for providing financial assistance for travel.

References

Barker, H. W., 1991: *Solar radiative fluxes for realistic extended broken cloud fields above reflecting surfaces*. Ph.D. thesis, McMaster University, 257 pp.

Barker, H. W and J. A. Davies, 1992: Solar radiative fluxes for stochastic, scale-invariant broken cloud fields. *J. Atmos. Sci.*, **49**, 1115-1126.

Barker, H. W., J. -J Morcrette, and G. D. Alexander, 1998: Broadband solar fluxes and heating rates for atmospheres with 3D broken clouds. *Q. J. R. Meteorol. Soc.*, **124**, 1245-1271.

Fu, Q. and K. -N. Liou, 1992: On the correlated-k distribution method for radiative transfer in inhomogeneous atmospheres. *J. Atmos. Sci.*, **49**, 2139-2156.

Joseph, J. H., W. J. Wiscombe, and J. A. Wienman, 1976: The delta-Eddington approximation for radiative transfer. *J. Atmos. Sci.*, **33**, 2452-2459.

Marshak, A., A. B. Davis, W. J. Wiscombe, and R. F. Cahalan, 1995: Radiative smoothing in fractal clouds. *J. Geophys. Res.*, **100**, 26247-26261.